Article

Magnetically Recoverable ICT-Functionalized Fe_3O_4 Nanoparticles for Efficient Horseradish Peroxidase Immobilization

Katarina Isaković , Marko Jonović , Dušan Sredojević * , Marko Bošković , Jovana Periša , Zorica Knežević-Jugović , Vesna Lazić *

Posted Date: 5 December 2025

doi: 10.20944/preprints202512.0446.v1

Keywords: 5-aminosalicylic acid (5ASA); enzyme immobilization; Fe_3O_4 nanoparticles; horseradish peroxidase (HRP); interfacial charge transfer (ICT)

 doi:10.20944/preprints202512.0446.v1

Article

Magnetically Recoverable ICT-Functionalized Fe_3O_4 Nanoparticles for Efficient Horseradish Peroxidase Immobilization

Katarina Isaković [1], Marko Jonović [2], Dušan Sredojević [1,*], Marko Bošković [3], Jovana Periša [1], Zorica Knežević-Jugović [4] and Vesna Lazić [1,*]

[1] Vinča Institute of Nuclear Sciences, National Institute of the Republic of Serbia, Centre of Excellence for Photoconversion, University of Belgrade, Belgrade, Serbia
[2] Institute of Chemistry, Technology and Metallurgy, University of Belgrade, Belgrade, Serbia
[3] Vinča Institute of Nuclear Sciences, National Institute of the Republic of Serbia, University of Belgrade, Belgrade, Serbia, Laboratory for Theoretical and Condensed Matter Physics, Serbia
[4] Department of Biochemical Engineering and Biotechnology, Faculty of Technology and Metallurgy, University of Belgrade, Belgrade, Serbia
* Correspondence: dusanmcrae@yahoo.com (D.S.); vesna.lazic@vin.bg.ac.rs (V.L.)

Abstract

The formation of interfacial charge transfer (ICT) complexes between phenolic ligands and metal oxide surfaces enables surface functionalization strategies with potential applications in catalysis and bioconjugation. In this study, magnetite (Fe_3O_4) nanoparticles were modified with two phenolic ligands, 5-aminosalicylic acid (5ASA) and caffeic acid (CA), to generate ICT complexes capable of covalent or non-covalent enzyme immobilization, respectively. The modified nanomaterials were structurally characterized using X-ray diffraction (XRD), transmission electron microscopy (TEM), and Fourier-transform infrared spectroscopy (FTIR). Horseradish peroxidase (HRP) was immobilized on these functionalized supports. Catalytic activity was evaluated using pyrogallol oxidation assays, with systematic variations in nanoparticle mass and enzyme concentration. The Fe_3O_4/5ASA–HRP system exhibited a maximum activity of 2.5 U per 20 mg of support (approximately 125 U/g), whereas Fe_3O_4/CA showed minimal activity under the same conditions. Data from enzyme loading studies confirmed that 5ASA-enabled covalent attachment resulted in significantly higher immobilization efficiency (up to 1068 mg/g) compared to the CA system. The magnetic properties of Fe_3O_4 allowed for rapid recovery of the biocatalysts using an external magnetic field. These results highlight the effectiveness of ICT-based functionalization for enzyme immobilization, positioning Fe_3O_4/5ASA as a promising platform for robust and reusable biocatalysts in environmental and industrial applications.

Keywords: 5-aminosalicylic acid (5ASA); enzyme immobilization; Fe_3O_4 nanoparticles; horseradish peroxidase (HRP); interfacial charge transfer (ICT)

1. Introduction

The development of interfacial charge transfer (ICT) complexes between phenolic compounds and metal oxide surfaces represents a powerful approach to extending absorption into the visible range, enabling novel photocatalytic and biomedical applications. ICT complexes form through covalent interactions between OH groups from phenolate ligands with OH groups on metal oxide nanoparticle surfaces [1–3]. This bonding induces a visible-range red shift in optical absorption, as energy from the phenolic donor is directly transferred to the semiconductor conduction band. In our previous studies, we successfully demonstrated the formation of ICT complexes between bioactive

 doi:10.20944/preprints202512.0446.v1

plant extracts and oxide surfaces, such as TiO_2, ZrO2, and CeO_2, leading to enhanced visible-light properties and biological functions [4–12].

Although Fe_3O_4 nanoparticles are intrinsically black and do not allow for straightforward detection of visible-light absorption shifts via UV/Vis spectroscopy, they possess a hydroxyl-rich surface highly suitable for interfacial charge transfer (ICT) complex formation. Phenolic ligands such as flavonoids or salicylic acid derivatives can form stable ICT complexes by coordinating through their phenolic –OH groups to surface Fe–OH moieties [7]. This interaction not only enhances chemical stability and anchoring of the ligands but also introduces additional functional groups to the nanoparticle interface [1,4,8,13]. For instance, in the case of 5-aminosalicylic acid (5ASA), while the phenolic –OH participates in ICT complex formation, the $–NH_2$ group on the opposite end remains accessible and reactive. This spatial orientation enables further surface modification or covalent attachment of biomolecules, such as enzymes. Therefore, ICT complexation with phenolic ligands serves not only as a surface engineering strategy but also as a platform for the multifunctionalization of Fe_3O_4 nanoparticles, including enzyme immobilization in biocatalysis and biomedical applications.

Immobilizing enzymes on nanoparticles harnesses advantages such as enhanced stability, easy recovery, reusability, and applicability in complex reaction environments. In addition to the well-established benefits of enzyme immobilization, nanocarriers offer an increased surface area for enzyme binding and enhanced reaction efficiency, further enhancing catalytic performance. While recovery of non-magnetic nanoparticles often requires advanced separation techniques, magnetic Fe_3O_4 nanoparticles may facilitate easier separation of immobilized enzymes.

Horseradish peroxidase (HRP), a heme-containing oxidoreductase, has been widely studied in this context and immobilized onto various nanosupports, including polymers, silica, and magnetic nanoparticles, using both physical adsorption and covalent attachment methods [14–20]. Early works demonstrated the physical adsorption of the enzyme onto unmodified Fe_3O_4 nanoparticles, resulting in increased thermal stability and retention of activity post-immobilization, although recovery was limited [15,19,21]. More advanced methods utilize covalent linking via glutaraldehyde or amine-functional silanes on Fe_3O_4–SiO_2 core–shell systems, resulting in enhanced loading, operational stability, and catalytic performance [18,22]. Recent reviews have highlighted the growing importance of magnetically recoverable carriers in enzyme immobilization, emphasizing their operational stability and suitability for industrial applications [23]. Techniques for oriented or tag-mediated immobilization on magnetic nanoparticles add another layer of control and efficiency [24]. Similarly, novel magnetic polymer platforms have demonstrated improved binding and durability in laccase immobilization [25]. In these systems, surface modification is achieved through a silica coating that is subsequently functionalized to introduce $–NH_2$ groups, which serve as anchoring points for enzyme conjugation. However, to the best of our knowledge, no study has reported a system where Fe_3O_4 nanoparticles are directly functionalized via interfacial charge transfer (ICT) complexation with small, naturally derived organic molecules to create a reactive surface suitable for covalent enzyme immobilization. This approach offers the advantage of combining surface stabilization, functional group specificity, and magnetic recoverability in a single-step modification strategy. Unlike conventional silica coating–amination methods, which require deposition of a silica layer followed by silanization to introduce reactive groups, our ICT-based approach achieves direct functionalization of the Fe_3O_4 surface through strong metal oxide–ligand binding, reducing the number of synthetic steps, avoiding organic solvents, and employing biocompatible ligands in an entirely aqueous process.

In this work, we explore a novel approach that integrates ICT-complex design with enzyme immobilization by functionalizing Fe_3O_4 nanoparticles with 5-aminosalicylic acid (5ASA) and caffeic acid (CA), enabling covalent and non-covalent binding of the enzyme. Although the intrinsic black color of Fe_3O_4 could hinder direct monitoring of ICT-related optical changes, the successful surface modification was confirmed through structural characterization, including X-ray diffraction (XRD) and transmission electron microscopy (TEM) for nanoparticle morphology, and Fourier-transform infrared spectroscopy (FTIR) for analyzing the functional groups before and after enzyme

 doi:10.20944/preprints202512.0446.v1

immobilization. The immobilization efficiency of horseradish peroxidase (HRP) will be evaluated using both ligands, and enzymatic activity will be systematically studied by varying the enzyme-to-nanoparticle ratio and the initial enzyme concentration. Reusability tests will be assessed through multiple catalytic cycles. The aim is to develop magnetically retrievable and catalytically efficient nanobiocatalysts, with potential applications in biosensing, green catalysis, and wastewater treatment.

2. Results and Discussion

2.1. Synthesis and Characterization of Fe_3O_4 Nanoparticles

The wide-angle XRD pattern of synthesized Fe3O4 nanoparticles is presented in Figure 1a. The diffractogram displayed the presence of several distinct peaks at 30.2, 35.6, 43.2, 53.7, 57.3, and 62.9° that belong to (220), (311), (400), (422), (511), and (440) planes of the inverse spinel crystalline Fe3O4, respectively (JCPDS Card No.85177).

Transmission electron microscopy (TEM) was used to perform a detailed morphological analysis of the Fe_3O_4 nanoparticles. As shown in the low-magnification TEM images (Figures 1c and 1d), the sample contained predominantly spherical nanoparticles with diameters of approximately 10 nm and rod-like structures measuring roughly 100 nm in length and 5 nm in width. The coexistence of spherical and rod-shaped nanoparticles is likely a consequence of the different iron salts, surfactants, or solvents used during the synthesis process [26,27]. Elemental analysis performed using energy-dispersive X-ray spectroscopy (EDX) (Figure 1b) confirmed the presence of iron as the primary component, along with oxygen and carbon, following the composition of the synthesized nanocomposite. Copper signals detected in the EDX spectrum originated from the copper grid used for sample mounting.

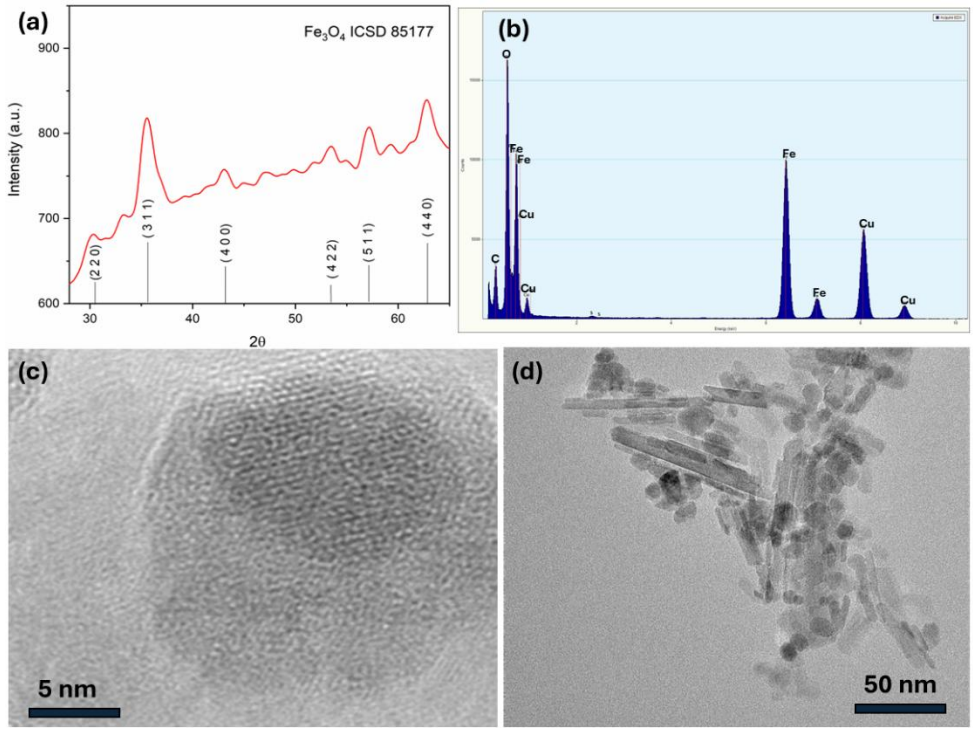

Figure 1. Characterization of Fe_3O_4 nanoparticles: **(a)** XRD pattern, **(b)** EDX spectrum, **(c)** and **(d)** high-magnification TEM images.

2.2. Immobilization of HRP to Fe_3O_4/5ASA and Fe_3O_4/CA Nanocomposite Materials

At the operational pH of 8.5, the enzyme peroxidase is immobilized onto the surface of Fe_3O_4 nanoparticles modified with 5ASA. Since the amino group of 5ASA has a pKa value of 5.8, it is

 doi:10.20944/preprints202512.0446.v1

deprotonated at this pH, which favors nucleophilic attack on carboxylate groups of Glu and Asp residues in the enzyme. This suggests that the enzyme is covalently bonded to the Fe_3O_4/5ASA surface via the formation of amide bonds between the $–NH_2$ groups of 5ASA and the carboxylate groups of *Glu* and *Asp* residues (Scheme 2a). The catalytic concentration of ferric and ferrous ions in the buffer solution may promote the formation of the amide bond [1]. On the other hand, the peroxidase enzyme cannot be immobilized onto the Fe_3O_4 NPs modified by caffeic acid (CA), likely due to the absence of covalent interactions. Instead, the enzyme is assumed to bind non-covalently to the surface $-COO^-$ groups of CA through hydrogen bonds and salt bridges (Scheme 2b). Hydrogen bonding can occur through amino acid residues such as Arg, His, Lys, and Cys, among others. At the same time, salt bridges may be formed between CA and *Arg*, *Lys*, and *Pro* residues that are protonated in the buffer solution (pH = 8.5). This could explain why the enzymes cannot form covalent bonds with Fe_3O_4/CA NPs. Since these residues have high pKa values (12.5, 10.8, and 10.6, respectively), they remain protonated at this pH, which prevents nucleophilic attack and thus the formation of amide bonds with CA.

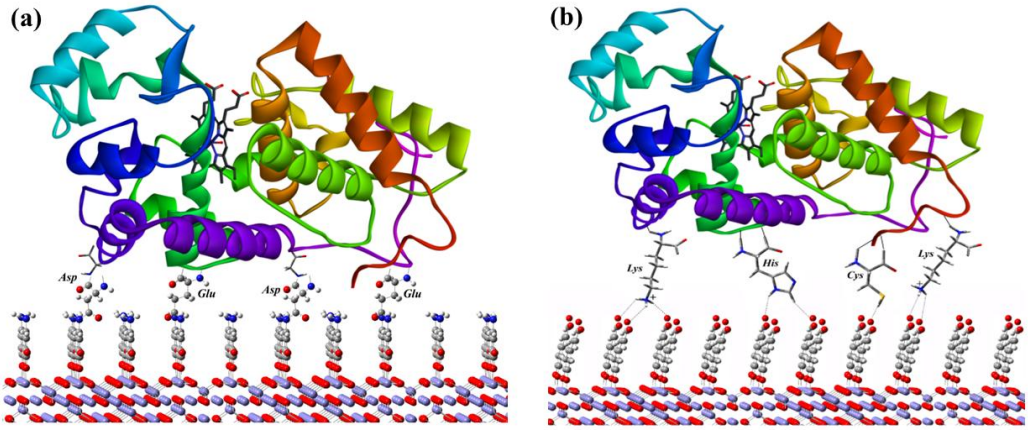

Scheme 2. Enzyme peroxidase is pictorially represented as immobilizing on the surface of Fe_3O_4 nanoparticles modified with **(a)** 5ASA and **(b)** CA. The amide bonds between the amino groups of 5ASA and the amino acid residues of *Glu* and *Asp* are indicated. The interactions between the COO groups of CA and the amino acid residues of *Lys, His, and Cys* are denoted with dotted lines. (gray: carbon; white: hydrogen; red: oxygen; blue: nitrogen; yellow; sulfur; purple: iron).

FTIR analysis was conducted better to characterize the interactions between HRP and functionalized Fe_3O_4 nanoparticles, and the results are presented in Figure 2 **(a)** Fe_3O_4/5ASA and **(b)** Fe_3O_4/CA). The absorption peak at 580 cm^{-1} was the vibration of the Fe–O bond [28,29].

Figure 2 shows the FTIR spectra of the Fe_3O_4 nanoparticles, free ligands (CA and 5ASA), the enzyme HRP, and corresponding hybrid materials before and after immobilization. The absorption peak at 560 cm^{-1} was the vibration of the Fe–O bond [28]. The peaks between 3000 and 3500 cm^{-1} are due to the O-H stretching vibration from hydroxyl groups on nanomaterials [30]. The FTIR absorption spectrum of the 5ASA is shown in Figure 2a. Notably, a band of average intensity at 1647 cm^{-1} corresponds to the asymmetric stretch of the C=O bond and bands of intensity at 1446 cm^{-1} and 1485 cm^{-1} corresponding to the angular and axial deformations of the C–O–H and stretches of the aromatic ring C=C bonds, respectively, confirming the presence of a carboxylic group in the chemical structure of the 5ASA [31]. The bands at 1574 and 1263 cm^{-1}, assigned to N–H vibrations, almost disappear after enzyme immobilization, suggesting that the amino group participates in amide bond formation with the enzyme. The HRP spectrum itself displays characteristic C–N and C=O stretching bands, which partially overlap with those of the Fe_3O_4/5ASA/HRP composite, confirming enzyme binding on the nanoparticle surface. The FTIR absorption spectrum of the CA is shown in Figure 2b. Bands at 2982 and 2912 cm^{-1} are ascribed to the C-H vibration modes [32]. The nanomaterial modified

 doi:10.20944/preprints202512.0446.v1

with caffeic acid exhibits a carbonyl-associated peak in all three samples, both before and after enzyme immobilization, suggesting that no covalent bonding occurred between the enzyme and the material. The intense band at 1645 cm^{-1} is assigned to the stretching of the carbonyl group (C=O) from the CA. Furthermore, the intense bands at 1450 cm^{-1} are attributed to olefinic C-C stretching modes.

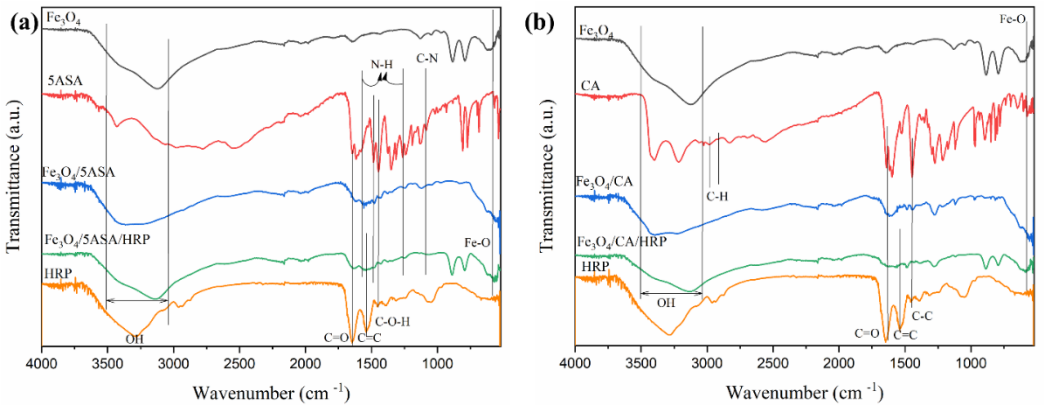

Figure 2. FTIR spectra of Fe_3O_4 nanoparticles and composite nanomaterials **(a)** Fe_3O_4/5ASA and **(b)** Fe_3O_4/CA before and after immobilization with HRP.

The magnetization curves of Fe_3O_4, Fe_3O_4/CA, and Fe_3O_4/5ASA before and after HRP enzyme immobilization were measured at 300 K in a magnetic field range of -50 to +50 kOe, as shown in Figure 3. The saturation magnetization of pristine Fe_3O_4 was 45 emu/g. After functionalization with caffeic acid and 5-aminosalicylic acid, the saturation magnetization values slightly decreased to 40 emu/g (Fe_3O_4/CA) and 41 emu/g (Fe_3O_4/5ASA), which can be attributed to the presence of a non-magnetic organic phase on the surface of the magnetic nanoparticles. Upon enzyme immobilization, a further reduction in magnetization was observed for the Fe_3O_4/5ASA sample (37 emu/g), consistent with the increased proportion of non-magnetic material resulting from the enzyme's presence. In contrast, the Fe_3O_4/CA sample exhibited a small increase in saturation magnetization after immobilization (43 emu/g). This may be due to partial loss or destabilization of the organic layer during the immobilization process, which was conducted at pH 8.5, potentially affecting the overall mass composition of the hybrid material. These variations in magnetization values reflect the relative contribution of magnetic versus non-magnetic components within the total composite mass and are consistent with expectations for organic-inorganic hybrid nanostructures [33].

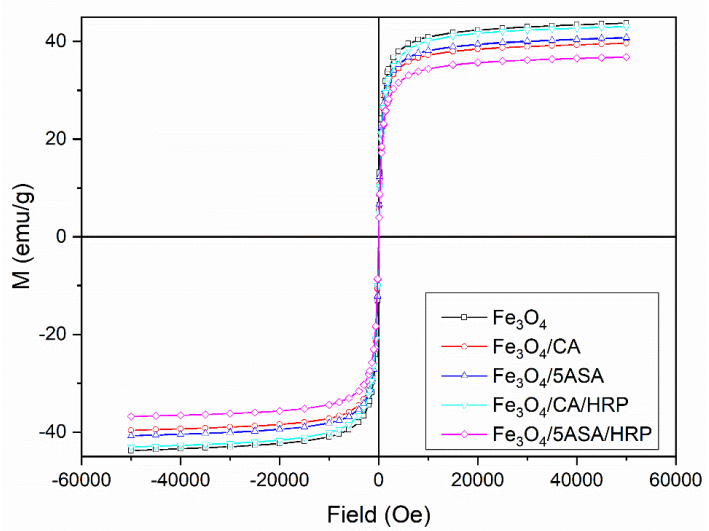

Figure 3. Magnetization curves of Fe_3O_4, Fe_3O_4/CA, and Fe_3O_4/5ASA before and after immobilization with HRP.

 doi:10.20944/preprints202512.0446.v1

2.3. Activity of HRP Immobilized to Fe_3O_4/5ASA and Fe_3O_4/CA Nanocomposite Materials

The results presented in Figure 4 clearly show that HRP immobilized on Fe_3O_4/5ASA nanomaterials exhibited significantly higher catalytic activity than that on Fe_3O_4/CA under all tested conditions. For the condition with 10 mg of nanoparticles (Figure 4a, left set), activity increased with enzyme concentration, reaching its highest value at 187.5 μg/mL. Activity increases slightly with a higher concentration of the enzyme (250 μg/mL). This effect is consistent with the non-monotonic loading-activity relationship often observed for immobilized enzymes: excessive surface coverage can cause steric crowding and shielding of active sites, increase diffusional limitations, and promote partial inactivation upon exposure to H_2O_2 [34]. Even with this decrease at 250 μg/mL, the highest measured value for Fe_3O_4/5ASA (2.5 U with 20 mg of nanoparticles) corresponds to over 125 U/g of nanomaterial, indicating excellent catalytic performance after immobilization. This superior activity can be attributed to the covalent bonding between HRP and the 5-aminosalicylic acid-modified surface, which likely creates a stable and favorable microenvironment for the enzyme, limiting conformational changes and preventing leaching during washing and reuse. In contrast, caffeic acid (CA)-functionalized nanoparticles enable only non-covalent interactions (e.g., hydrogen bonding, ionic bridges), which are less stable under operational conditions, as reflected by both the low initial activity (max 0.08 U) and the rapid loss in performance upon repeated use. The low activity of the Fe_3O_4/CA system can be attributed to the molecular orientation of caffeic acid on the Fe_3O_4 surface, where –COOH groups remain exposed and do not participate in covalent coupling with the enzyme. As a result, HRP is bound predominantly through weak non-covalent interactions such as hydrogen bonding and ionic bridges, leading to reduced catalytic stability under operational conditions. Data from Table S1 further support these findings: for Fe_3O_4/5ASA, the amount of immobilized enzyme reached up to 1068.7 mg/g of support, with 21.4 mg of HRP retained on 20 mg of nanoparticles, while a substantial portion of the enzyme remained in the reaction mixture when CA-functionalized materials were used, typically under 5 mg/g, with most values falling below the detection limit. For these samples, enzyme loading was at or below the Bradford assay detection limit, and in some cases could not be quantified with confidence (reported as ND in Table S1). This pronounced difference demonstrates that 5ASA-functionalization not only promotes covalent binding but also facilitates substantially higher enzyme loading, directly contributing to enhanced catalytic performance.

Although literature values for HRP activity expressed in U/g of support are scarce, similar systems employing covalent immobilization strategies, such as HRP on modified silica or synthetic polymer beads, report activity in the range of 200–800 U/g [35,36], depending on enzyme loading and surface properties. Therefore, the achieved values in this study are comparable or superior to many existing immobilization systems, particularly considering the simplicity of the Fe_3O_4-based platform and the mild immobilization conditions employed. These results highlight the importance of rational surface functionalization and immobilization chemistry in designing nanomaterials that retain or even enhance the catalytic activity of enzymes after attachment.

The results shown in Figure 5 demonstrate that HRP immobilized on Fe_3O_4/5ASA nanomaterials exhibits only a moderate decrease in activity after the first two catalytic cycles (approximately 10% loss for 10 mg, 20% loss for 15 mg, 25% loss for 20 mg of nanoparticles). For 30 mg of nanoparticles, the activity decreases by about 50% after the second cycle. The sharp initial decrease, pronounced after the first cycle, likely results from the removal of loosely adsorbed or weakly bound enzyme molecules during washing and reaction. At the same time, the subsequently retained activity reflects the fraction of the enzyme covalently attached to the support. Afterward, a more gradual decline of up to ~80% is observed from the third cycle onward, indicating progressive inactivation of the firmly bound enzyme fraction. This loss is attributed to partial enzyme inactivation resulting from repeated exposure to hydrogen peroxide and pyrogallol, which leads to oxidative damage of the heme group and nearby amino acids, as well as potential conformational changes induced by the reaction conditions. Additionally, gradual blocking of active sites by oxidation products may further contribute to activity loss. Nevertheless, the residual activity obtained after five cycles remains higher than that of the Fe_3O_4/CA system and several non-covalent immobilization platforms reported in the

 doi:10.20944/preprints202512.0446.v1

literature [37,38], confirming the competitive stability of the Fe_3O_4/5ASA nanobiocatalysts. This high level of operational stability was particularly observed for nanobiocatalysts prepared using higher amounts of nanoparticles (20–30 mg) during the immobilization step, i.e., at a lower enzyme-to-nanocarrier ratio, indicating that improved enzyme distribution and reduced surface crowding contribute to better performance after the initial washout of weakly bound enzyme. The enhanced performance is attributed to covalent bonding between the enzyme and the amino-functionalized surface of the nanoparticles, which likely stabilizes the enzyme structure and prevents leaching. In addition to the high catalytic activity and stability observed, the Fe_3O_4/5ASA system offers several practical advantages over many reported immobilization platforms, including the formation of a stable ICT complex with covalent metal oxide-ligand binding, a simple and reproducible functionalization procedure performed entirely in aqueous medium without generating unnecessary waste, and the use of biocompatible ligands, making the process environmentally friendly and suitable for potential biomedical applications. In contrast, HRP immobilized on Fe_3O_4/CA, where only non-covalent interactions are present, shows a rapid decline in activity, losing approximately 90% of its initial value after only two cycles. When explicitly compared with other magnetic nanoparticle-based immobilization systems reported in the literature, these results confirm that covalent immobilization via 5-aminosalicylic acid provides not only high initial activity (as shown in Figure 4) but also maintains a competitive absolute activity level after multiple reuses, making this system highly promising for biotechnological applications requiring robust and reusable biocatalysts.

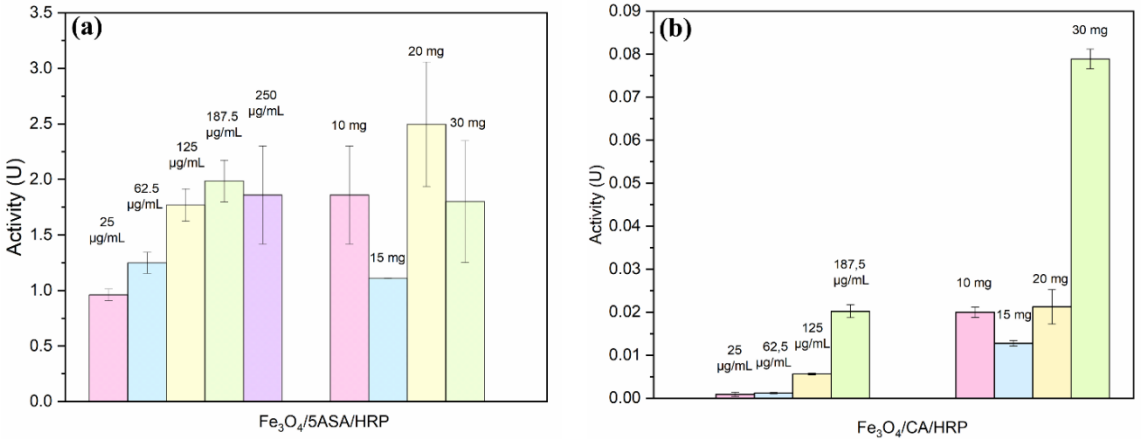

Figure 4. Enzyme activity (U) of HRP immobilized on **(a)** Fe_3O_4/5ASA and **(b)** Fe_3O_4/CA. Left bars: varying enzyme concentrations (25–250 µg/mL) with 10 mg of nanoparticles. Right bars: varying nanoparticle amounts (10–30 mg) with 250 µg/mL of enzyme.

From a practical perspective, the proposed functionalization and immobilization strategy is well-suited for scaling up, as it is based on a single-step aqueous process, utilizes inexpensive and biocompatible ligands, and avoids the use of organic solvents or specialized equipment. The magnetic nature of the carriers enables rapid and straightforward separation from the reaction media using an external magnetic field, which is particularly advantageous in both continuous and batch processes. As shown in Figure 5, the Fe_3O_4/5ASA nanobiocatalysts retain a high absolute activity even after five reuse cycles, despite a decline over time, suggesting that the system can maintain satisfactory performance in extended operations. Potential limitations for industrial application include partial activity loss after multiple cycles, the need to optimize nanoparticle dispersion to minimize agglomeration in larger volumes, and the cost of enzyme replenishment. These aspects can be addressed in future studies through process optimization, improved immobilization chemistries, or enzyme engineering, paving the way for pilot-scale and industrial implementation.

 doi:10.20944/preprints202512.0446.v1

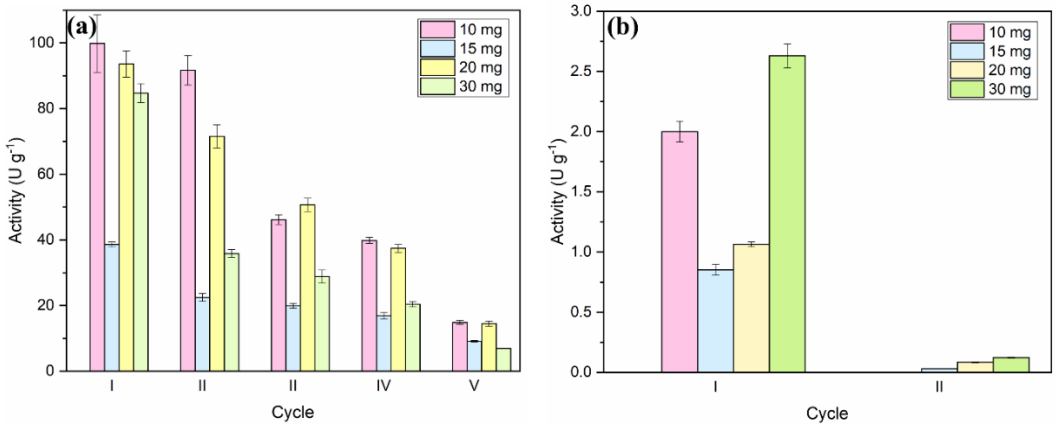

Figure 5. Activity in cycles of peroxidase immobilized on **(a)** Fe_3O_4/5ASA nanoparticles and **(b)** Fe_3O_4/CA nanoparticles vs. different amounts of nanoparticles used during the immobilization, with 250 μg/mL of enzyme.

Figure 6 illustrates how varying the initial enzyme concentration affects the catalytic durability of HRP immobilized on Fe_3O_4/5ASA and Fe_3O_4/CA supports over five reuse cycles. In the Fe_3O_4/5ASA system, all tested concentrations maintained relatively high activity during the first two to three cycles, indicating that the enzyme molecules covalently attached to the 5ASA-functionalized surface remain structurally stable under reaction conditions. A significant decrease in activity was observed at higher enzyme concentrations (e.g., 187.5 μg/mL), where activity dropped by about 85% after five cycles. In contrast, samples prepared with moderate enzyme loadings (62.5-125 μg/mL) retained 40-50% of their activity even after four cycles, suggesting that lower initial enzyme concentrations provide better long-term stability. This trend likely results from reduced steric crowding and more uniform surface distribution of the enzyme, which minimizes conformational stress and facilitates substrate diffusion. Conversely, higher enzyme concentrations yield the highest initial activity but also greater susceptibility to inactivation during repeated use. The Fe_3O_4/CA system, on the other hand, exhibited a much faster decline in activity across all tested concentrations, losing most of its catalytic efficiency after only two cycles. This behavior reflects the weaker, non-covalent nature of enzyme binding in CA-functionalized materials and confirms the superior stabilization achieved via covalent immobilization through 5ASA.

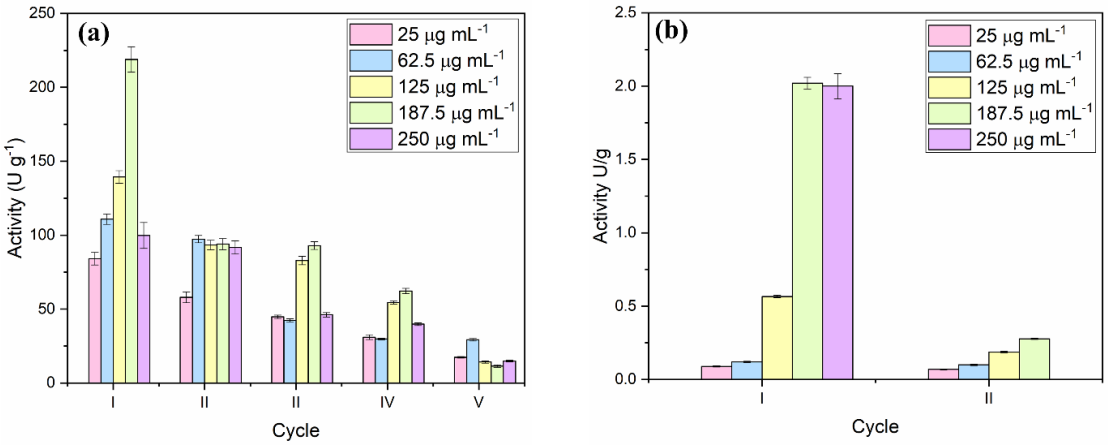

Figure 6. Activity in cycles of peroxidase immobilized on **(a)** Fe_3O_4/5ASA nanoparticles and **(b)** Fe_3O_4/CA nanoparticles vs. different concentrations of enzyme, with 10 mg of material.

When compared with relevant literature, the Fe_3O_4/5ASA system demonstrates competitive performance. HRP immobilized on mesoporous magnetic silica supports retained about 70% of its activity after ten cycles [37], while ceramic-based composites maintained around 66% after ten uses

 doi:10.20944/preprints202512.0446.v1

[39]. Moreover, an HRP-mesoporous composite exhibited just 50% activity after five cycles, illustrating significant enzyme loss [40]. In our system, although a gradual loss of activity occurs with repeated use, Fe_3O_4/5ASA–HRP prepared with moderate enzyme concentrations (62.5–125 μg/mL) retains 40–50% of its activity even after four cycles, which is comparable to or higher than that of many reported magnetic nanocarriers under similar conditions. This stability, combined with the simplicity of the functionalization procedure and the biocompatible nature of 5ASA, highlights the potential of this system for applications where reusability and environmental safety are critical, even if partial enzyme deactivation occurs over multiple cycles.

The excellent catalytic performance of Fe_3O_4/5ASA/HRP was further supported by reusability experiments (Figures 5 and 6), which demonstrated that both the amount of nanomaterial and the initial enzyme concentration play crucial roles in operational stability. Increasing the quantity of nanoparticles (Figure 5) led to a slower decline in activity, with the highest stability observed at 20-30 mg, where activity loss after five cycles was notably lower than at smaller nanoparticle amounts. Varying the initial enzyme concentration (Figure 6) revealed that, although all Fe_3O_4/5ASA samples retained high activity in the first few cycles, the sample with the loading of 187.5 μg/mL experienced a nearly 85% decrease after five consecutive cycles. In contrast, lower initial enzyme concentrations showed more minor losses after four cycles, suggesting that lower loading may be advantageous when extended reuse is required, while higher loading is beneficial when maximal initial activity is prioritized for short-term applications. This behavior likely reflects differences in enzyme packing density and active site accessibility, as well as the impact of oxidative stress and product accumulation during repeated use. In contrast, Fe_3O_4/CA-based systems exhibited a sharp decline in activity across all conditions, indicating that non-covalent binding is insufficient to provide stability under operational stresses. Together, these findings confirm that covalent immobilization via 5ASA not only enables high catalytic activity but also provides a tunable strategy for balancing immediate performance and long-term operational stability, critical parameters for practical biocatalytic applications.

3. Materials and Methods

HRP enzyme (EC 1.11.1.7; donor: H2O2 oxidoreductase) with a specific activity of 250 purpurogallin units per mg, pyrogallol, 2-mercaptoethanol, and iron (II) sulfate heptahydrate were obtained from Sigma-Aldrich (St. Louis, MO, USA). Hydrochloric acid 37% was obtained from Acros Organic (New Jersey, USA). Iron (III) chloride hexahydrate was obtained from Carlo Erba Reagents S.A.S. (France). Hydrogen peroxide (H2O2) 3% (0.97 M) was purchased from Galafarm (Belgrade, Serbia). Sodium dihydrogen phosphate, disodium hydrogen phosphate, and acetic acid were obtained from Centrohem (Stara Pazova, Serbia). 1-ethyl-3-(3-dimethylaminopropyl) carbodiimide (EDAC) was obtained from Thermo Fisher Scientific (Waltham, MA, USA). Ammonium hydroxide was obtained from NPK Engineering (Belgrade, Serbia). 5-aminosalicylic acid and pyrogallol were obtained from Alfa Aesar (Karlsruhe, Germany), while caffeic acid was obtained from TCI Development Co. (Shanghai, China). Other chemicals used in this work were of commercial analytical grade. Milli-Q deionized water was used as the solvent with a resistivity of 18.2 MΩ cm−1.

3.1. Synthesis of Magnetic Nanoparticles

Fe_3O_4 nanoparticles were synthesized using a co-precipitation method in which ammonium hydroxide (NH_4OH) served as the precipitating agent [7]. In this procedure, $FeCl_3$ and $FeSO_4$ were co-precipitated with a 10% excess of Fe^{2+} to compensate for partial oxidation of Fe^{2+} to Fe^{3+} during synthesis, which can occur in the presence of dissolved oxygen. This excess ensures that the required stoichiometric Fe^{2+}:Fe^{3+} ratio of 1:2 is maintained throughout the reaction, allowing for the formation of phase-pure magnetite with optimal magnetic properties. For every experiment, 13.5 g of $FeCl_3 \cdot 6H_2O$ and 7.65 g of $FeSO_4 \cdot 7H_2O$ were dissolved in 20 mL of distilled water. The precipitation was carried out at room temperature (22–24 °C) under continuous vigorous magnetic stirring (~800 rpm). Concentrated ammonium hydroxide (25% NH_4OH, 17 mL) was added dropwise to the iron

 doi:10.20944/preprints202512.0446.v1

salt solution, with continuous monitoring of the pH using a calibrated pH meter to maintain a pH of approximately 11 during the precipitation process. The resulting mixture was then diluted with distilled water to reach a total volume of 150 mL while stirring for approximately 30 minutes. The solid product was separated from the reaction mixture using a strong magnetic field and washed repeatedly with 1000 mL of distilled water (over 7–8 cycles) until the pH stabilized at around 7. Subsequently, the washed magnetite powder was redispersed in 100 mL of distilled water, and the pH was adjusted to 2 to promote peptization. The colloidal dispersion was dialyzed against a 1 mM HCl solution until the pH settled at approximately 3, and then it was stored overnight at 4 °C in a refrigerator. Finally, the colloidal magnetite was transferred into a volumetric flask and stored in the dark at 4 °C for further use. Afterward, the dispersion was dried in an oven at 45 °C before characterization and functionalization. Representative photographs of the synthesis steps are shown in Figure S1a–d (Supporting Information).

3.2. Preparation of Fe_3O_4 with 5-Aminosalicylic and Caffeic Acid

The appropriate ligands (89 mg of 5ASA and 104,8 mg of CA) were dissolved under continuous stirring using a magnetic stirrer with gentle heating (50 mL of distilled water per 100 mg of Fe_3O_4). After the complete dissolution of the ligands, magnetic nanoparticles were introduced into the solution (in a molar ratio of Fe_3O_4 to ligands of 1:1.35) and incubated at room temperature in the dark for three days. The ligand-to-Fe_3O_4 molar ratio of 1:1.35 was selected based on the estimated density of surface –OH groups (~10 groups per nm^2) calculated from the specific surface area of the nanoparticles, as determined in our previous studies [7]. This amount provides sufficient ligand to achieve complete surface coverage without introducing excess unbound ligand. After incubation, the dispersion was transferred into a cuvette and thoroughly mixed with deionized water using a vortex mixer to facilitate washing and removal of any unbound ligand. The nanoparticles were then separated first by applying a strong magnet and subsequently by centrifugation to collect the precipitate. This washing/separation cycle was repeated at least three times. The supernatant was removed, and the remaining sample was dried at 40 °C.

3.3. Nanoparticle Activation and HRP Immobilization

The nanomaterials were treated with 22 mg of EDAC in 18 mL of Tris-HCl buffer (50 mM, pH 8.5) for 30 minutes at 25 °C under gentle stirring (150 rpm) to activate Fe_3O_4 nanomaterials, following the optimized procedure from our previous work [22]. These parameters, including EDAC concentration, activation time, and pH, were selected to ensure a strong covalent attachment of the enzyme and high retention of activity. The chosen pH of 8.5 provides a balance between maintaining HRP structural stability and ensuring deprotonation of the amino groups of 5ASA (pKa ≈ 5.8), which promotes nucleophilic attack on the enzyme's carboxyl groups and enables amide bond formation. Afterward, 10, 25, 50, 75, or 100 µL (depending on whether the amount of particles or enzyme is varied) of HRP solution was added to a vessel containing 10, 15, 20, and 30 mg of activated nanomaterials, along with 990, 975, 950, 925 or 900 µL of Tris-HCl buffer (50 mM, pH 8.5), 1 mL od EDAC in final immobilization volume of 2 mL. Immobilization was performed for 20 hours at 25 °C under gentle stirring (150 rpm). The main stages of the immobilization process are depicted in Figure S1e (Supporting Information).

The schematic representation of the immobilization process is shown in Scheme 1. It illustrates the formation of an interfacial charge transfer (ICT) complex between Fe_3O_4 and (a) 5-aminosalicylic acid (5ASA), followed by the covalent binding of horseradish peroxidase (HRP) via the free amino group of 5ASA, or (b) caffeic acid (CA).

 doi:10.20944/preprints202512.0446.v1

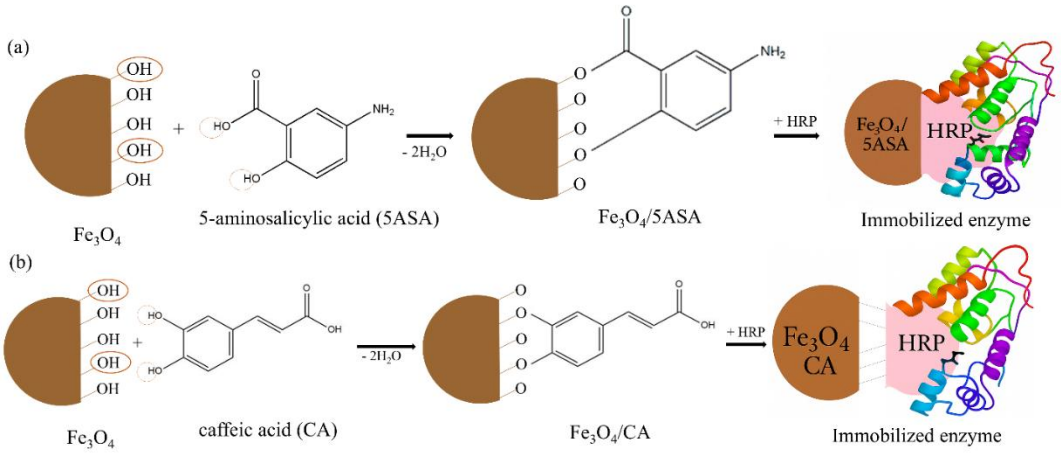

Scheme 1. Schematic illustration of the immobilization of horseradish peroxidase (HRP) onto Fe_3O_4 nanoparticles functionalized with (a) 5-aminosalicylic acid (5ASA) via interfacial charge transfer (ICT) complex formation and covalent binding through the amino group of 5ASA (b) caffeic acid (CA) via interfacial charge transfer (ICT) complex formation and hydrogen binding with CA.

3.4. Determination of Protein Concentration Using the Bradford Method

Immobilization efficiency (mg/g) was calculated as the difference between the initial amount of enzyme added to the reaction mixture and the amount remaining in the supernatant after immobilization, divided by the dry mass of the nanomaterial (g). The amount of enzyme in both the initial and final solutions was determined using the Bradford assay. Protein concentration was determined using the Bradford assay reagent, prepared from Coomassie-Brilliant Blue G-250 according to standard protocols [22]. Briefly, 40 µL of the sample was mixed with 2 mL of diluted dye reagent, and absorbance was measured after incubation. The dye reagent was prepared in-house by diluting a concentrated Coomassie Brilliant Blue G-250 solution, following the established procedure. The concentration of the enzyme in solution was determined both before and after the immobilization process using the described method. The difference in enzyme concentration was then calculated per gram of nanomaterial.

3.5. Determination of Enzyme Activity

The enzymatic activity of immobilized horseradish peroxidase (HRP) was assessed using pyrogallol as the standard substrate in the presence of hydrogen peroxide (H_2O_2). The reaction was monitored spectrophotometrically at 420 nm, corresponding to the formation of purpurogallin—the oxidative product of pyrogallol. The assay was conducted using a UV-Vis spectrophotometer (UV-1700, Shimadzu Corporation, Kyoto, Japan), which detected the color change from yellow (pyrogallol) to dark violet-brown (purpurogallin).

The reaction mixture consisted of 13 mM pyrogallol in 0.1 M phosphate buffer (pH 7.0), 3% (v/v) hydrogen peroxide, and varying quantities (10, 15, 20, or 30 mg) of HRP-immobilized magnetic nanoparticles. A blank control was prepared using the same pyrogallol solution in phosphate buffer without adding hydrogen peroxide. The absorbance of the reaction mixture was recorded every 15 seconds over 3 minutes, with measurements taken relative to the blank.

The total enzyme activity expressed in U is determined based on the following expression:

$$A_{IE} = \frac{\Delta A \times V_t}{\Delta t \times \varepsilon} \qquad (1)$$

$\frac{\Delta A}{\Delta t}$ – absorbance change per minute,

ε – the molar extinction coefficient of pyrogallol at 420 nm (12 L mmol $^{-1}$)

V_t – total volume of the reaction mixture (mL)

 doi:10.20944/preprints202512.0446.v1

The specific activity of the immobilized enzyme (Ug $^{-1}$) was calculated relative to the mass of the nanoparticle carrier. One unit (1 U) of peroxidase activity was defined as the amount of enzyme that catalyzes the oxidation of 1 μmol of pyrogallol to purpurogallin per minute under the assay conditions (25 °C, pH 7.0). The activity was calculated from the change in absorbance at 420 nm using the molar extinction coefficient of purpurogallin (ε = 12 L mmol^{-1} cm^{-1}). Representative photographs of the experimental setup and assay are provided in Figure S1f–h (Supporting Information). Reusability was assessed by magnetically separating the nanobiocatalyst after each cycle, washing it with deionized water, and reusing it under identical assay conditions for up to five consecutive runs.

All experiments were performed in triplicate, and results are expressed as mean ± standard deviation (SD).

3.6. Characterization of Fe_3O_4 Nanomaterials

The XRD pattern of Fe_3O_4 nanoparticles was recorded using a Rigaku SmartLab diffractometer (Cu-$K\alpha_{1,2}$ radiation, λ = 0.1540 nm) in a 2θ range of 10 to 90° with a 0.02° step and 1° min^{-1} counting time. Fourier transform infrared (FTIR) spectroscopy measurements of the Fe_3O_4, Fe_3O_4/5ASA, and Fe_3O_4/CA hybrid nanomaterials were performed before and after enzyme immobilization using a Thermo Nicolet 6700 FTIR spectrometer.

High-resolution transmission electron microscopy (HRTEM) was used to investigate the morphology and fine structural characteristics of the synthesized materials. Analyses were conducted using an instrument operating at 300 kV with a LaB_6 cathode as the electron source, enabling a theoretical resolution of 1.7 Å. The system was equipped with a GATAN MULTISCAN CCD camera (model 794) and an energy-dispersive X-ray spectroscopy (EDS) module (INCA x-stream, Oxford Instruments). For sample preparation, the powders were ultrasonically dispersed in ethanol, and a small volume of the resulting dilute suspension was deposited onto a copper grid coated with holey carbon, followed by air-drying at room temperature.

Magnetic measurements were performed using an MPMS XL-5 SQUID magnetometer. Isothermal magnetic curves were measured at 300 K in the -50 kOe to 50 kOe magnetic field range.

4. Conclusions

In this study, horseradish peroxidase (HRP) was successfully immobilized onto Fe3O4 nanoparticles functionalized with 5-aminosalicylic acid (5ASA) and caffeic acid (CA), using a simple and efficient covalent coupling strategy. The Fe_3O_4/5ASA system enabled covalent binding of the enzyme, resulting in significantly higher immobilization efficiency, catalytic activity (>100 U/g), and operational stability compared to the non-covalently bound Fe_3O_4/CA system. The Fe_3O_4/5ASA nanobiocatalysts maintained a competitive activity level after five reuse cycles, with the residual activity still surpassing that of the initial Fe_3O_4/CA system and many non-covalent immobilization platforms reported in the literature. This highlights their robustness, operational stability, and suitability for applications requiring reusable biocatalysts. In addition to excellent stability and reusability, the magnetic properties of the Fe_3O_4-based carrier allow for rapid and efficient separation from reaction mixtures using an external magnetic field, making this system highly practical for repeated or continuous biocatalytic applications. These results confirm the crucial role of surface functionalization in preserving enzyme structure and function, and highlight the potential of 5ASA-modified Fe3O4 nanoparticles as a robust, magnetically recoverable, and reusable platform for enzyme immobilization in various biotechnological applications.

Supplementary Materials: The following supporting information can be downloaded at the website of this paper posted on Preprints.org.

Author Contributions: K.I: methodology, investigation. M.J.: investigation. D.S.: methodology, validation, data curation. M.B.: formal analysis J.P: formal analysis. Z.K.J.: writing—review and editing, conceptualization. V.L.:

 doi:10.20944/preprints202512.0446.v1

writing—original draft, conceptualization, supervision. All authors have read and agreed to the published version of the manuscript.

Acknowledgments: This work was supported by the Ministry of Science, Technological Development and Innovation of the Republic of Serbia (Contract Number: 451-03-136/2025-03/200017 and Contract Number: 451-03-136/2025-03/200135).

Conflicts of Interest: The authors declare that they have no known competing financial interests or personal relationships that could have appeared to influence the work reported in this paper.:

References

1. V. Lazić, J.M. Nedeljković, Catalysts 14 (2024).
2. J. Fujisawa, S. Kato, M. Hanaya, The Journal of Physical Chemistry C 127 (2023) 15300–15306.
3. J. ichi Fujisawa, S. Kato, M. Hanaya, Chem Phys Lett 827 (2023).
4. V. Lazić, J.M. Nedeljković, in: Nanomaterials Synthesis: Design, Fabrication and Applications, Elsevier, 2019, pp. 419–449.
5. D. Sredojević, S. Stavrić, V. Lazić, S.P. Ahrenkiel, J.M. Nedeljković, Physical Chemistry Chemical Physics 24 (2022) 16493–16500.
6. I. Smičiklas, J. Papan, V. Lazić, D. Lončarević, S.P. Ahrenkiel, J.M. Nedeljković, J Environ Chem Eng 5 (2017) 3759–3765.
7. V. Lazić, K. Mihajlovski, A. Mraković, E. Illés, M. Stoiljković, S.P. Ahrenkiel, J.M. Nedeljković, ChemistrySelect 4 (2019) 4018–4024.
8. V. Lazić, I. Smičiklas, J. Marković, D. Lončarević, J. Dostanić, S.P. Ahrenkiel, J.M. Nedeljković, Vacuum 148 (2018) 62–68.
9. V. Nikšić, A. Pirković, B. Spremo-Potparević, L. Živković, D. Topalović, J.M. Nedeljković, V. Lazić, Int J Mol Sci 26 (2025).
10. A. Zarubica, D. Sredojević, R. Ljupković, M. Randjelović, N. Murafa, M. Stoiljković, V. Lazić, J.M. Nedeljković, Sustain Energy Fuels 7 (2023) 2279–2287.
11. D. Sredojević, V. Lazić, A. Pirković, J. Periša, N. Murafa, B. Spremo-Potparević, L. Živković, D. Topalović, A. Zarubica, M. Jovanović Krivokuća, J.M. Nedeljković, Nanomaterials 12 (2022).
12. M.G. Miljković, V. Lazić, K. Banjanac, S.Z. Davidović, D.I. Bezbradica, A.D. Marinković, D. Sredojević, J.M. Nedeljković, S.I. Dimitrijević Branković, Int J Biol Macromol 114 (2018) 1216–1223.
13. Z. Barbieriková, M. Šimunková, V. Brezová, D. Sredojević, V. Lazić, D. Lončarević, J.M. Nedeljković, Opt Mater (Amst) 123 (2022).
14. H.M. Abdel-Mageed, Micro and Nano Systems Letters 13 (2025).
15. X. Xie, P. Luo, J. Han, T. Chen, Y. Wang, Y. Cai, Q. Liu, Enzyme Microb Technol 122 (2019) 26–35.
16. W.H. Abdulaal, Y.Q. Almulaiky, R.M. El-Shishtawy, Catalysts 10 (2020).
17. X. Gao, Q. Zhai, M. Hu, S. Li, Y. Jiang, Catal Sci Technol 11 (2021) 2446–2455.
18. Q. Chang, H. Tang, Molecules 19 (2014) 15768–15782.
19. S.A. Mohamed, M.H. Al-Harbi, Y.Q. Almulaiky, I.H. Ibrahim, R.M. El-Shishtawy, Electronic Journal of Biotechnology 27 (2017) 84–90.
20. C. Shi, J. Sheng, G. Si, Y. Li, Y. Shen, N. Gu, J Mater Sci Technol 161 (2023) 161–169.
21. M.R. Ladole, J.S. Mevada, A.B. Pandit, Bioresour Technol 239 (2017) 117–126.
22. M. Jonović, B. Jugović, M. Žuža, V. Đorđević, N. Milašinović, B. Bugarski, Z. Knežević-Jugović, Polymers (Basel) 14 (2022).
23. A.L. Gama Cavalcante, D.N. Dari, F. Izaias da Silva Aires, E. Carlos de Castro, K. Moreira dos Santos, J.C. Sousa dos Santos, RSC Adv 14 (2024) 17946–17988.
24. C. Castro-Hinojosa, S. Del Sol-Fernández, E. Moreno-Antolín, B. Martín-Gracia, J.G. Ovejero, J.M. de la Fuente, V. Grazú, R.M. Fratila, M. Moros, Bioconjug Chem 34 (2023) 2275–2292.
25. Y.Q. Almulaiky, J. Alkabli, R.M. El-Shishtawy, Int J Biol Macromol 282 (2024) 137362.
26. B. Mol, A.E. Beeran, P.S. Jayaram, P. Prakash, R.S. Jayasree, S. Thomas, B. Chakrapani, M.R. Anantharaman, M.J. Bushiri, J Mater Sci Mater Med 32 (2021).

 doi:10.20944/preprints202512.0446.v1

27. J. Mohapatra, M. Xing, J. Beatty, J. Elkins, T. Seda, S.R. Mishra, J.P. Liu, Nanotechnology 31 (2020) 275706.
28. H. Heryanto, D. Tahir, Ceram Int 47 (2021) 16820–16827.
29. S.H. Chaki, T.J. Malek, M.D. Chaudhary, J.P. Tailor, M.P. Deshpande, Advances in Natural Sciences: Nanoscience and Nanotechnology 6 (2015).
30. S.H. Chaki, T.J. Malek, M.D. Chaudhary, J.P. Tailor, M.P. Deshpande, Advances in Natural Sciences: Nanoscience and Nanotechnology 6 (2015).
31. J.G. Pontes-Neto, T.R.F. Silva, F.O.S. Ribeiro, D.A. Silva, M.F.R. Soares, J.L. Soares-Sobrinho, J Therm Anal Calorim 147 (2022) 3141–3149.
32. L. Vertuccio, L. Guadagno, A. D'Angelo, V. Viola, M. Raimondo, M. Catauro, Applied Sciences (Switzerland) 13 (2023).
33. C. Shi, J. Sheng, G. Si, Y. Li, Y. Shen, N. Gu, J Mater Sci Technol 161 (2023) 161–169.
34. F.B.H. Rehm, S. Chen, B.H.A. Rehm, Bioengineered 9 (2018) 6–11.
35. C.C. Chen, J.S. Do, Y. Gu, Sensors (Switzerland) 9 (2009) 4635–4648.
36. Y.-M. Lu, Q.-Y. Yang, L.-M. Wang, M.-Z. Zhang, W.-Q. Guo, Z.-N. Cai, D.-D. Wang, W.-W. Yang, Y. Chen, Clean (Weinh) 45 (2017) 1600077.
37. B. Bakar, M. Akbulut, F. Ulusal, A. Ulu, N. Özdemir, B. Ateş, ACS Omega 9 (2024) 24558–24573.
38. J. Rong, Z. Zhou, Y. Wang, J. Han, C. Li, W. Zhang, L. Ni, Food Technol Biotechnol 57 (2019) 260–271.
39. H.A. Salah, A.M. Elsayed, A.M. Abdel-Aty, G.A. Khater, A.A. El-Kheshen, M.M. Farag, S.A. Mohamed, Sci Rep 14 (2024).
40. M.N. El-Nahass, M.M. El-keiy, E.M.M. Ali, Int J Biol Macromol 116 (2018) 1304–1309.